JACS
JOURNAL OF THE AMERICAN CHEMICAL SOCIETY
Article
pubs.acs.org/JACS

Deposition of Ordered Layers of Tetralactam Macrocycles and Ether Rotaxanes on Pyridine-Terminated Self-Assembled Monolayers on Gold

Sebastian Richter,[†] Johannes Poppenberg,[†] Christoph H.-H. Traulsen,[†] Erik Darlatt,[‡] Anja Sokolowski,[†] Dominik Sattler,[†] Wolfgang E. S. Unger,*[,‡] and Christoph A. Schalley*[,†]

[†]Institut für Chemie und Biochemie, Freie Universität Berlin, Takustraße 3, 14195 Berlin, Germany

[‡]BAM-Bundesanstalt für Materialforschung und -prüfung, Unter den Eichen 44-46, 12203 Berlin, Germany

Supporting Information

ABSTRACT: The deposition of tetralactam macrocycles and the corresponding benzyl ether rotaxanes on gold substrates is investigated for the first time exploiting metallo-supramolecular chemistry. Two pyridine-terminated self-assembled monolayers (SAMs) are developed that are used as well-ordered template layers. The two SAMs differ with respect to the rigidity of the terminal pyridines as shown by angle-resolved near-edge X-ray absorption fine structure (NEXAFS) spectroscopy. The template layers are then used for the metal-mediated self-assembly of macrocylces and rotaxanes on solid supports. The SAM with the more rigid terminal pyridine shows a higher coverage with the macrocycles and is therefore preferable. Angle-resolved NEXAFS spectroscopy also shows the deposited supramolecules to be oriented preferentially upright. This order is only achieved for the macrocycles through the deposition on the more rigid SAM template, whereas rotaxanes form oriented layers on both SAMs. Time-of-flight secondary-ion mass spectrometry analysis was used to determine the deposition time required for the self-assembly process.

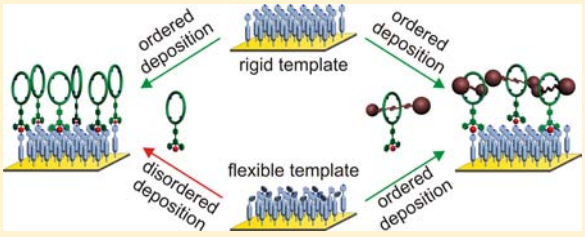

1. INTRODUCTION

In current nanotechnology research, the investigation of synthetic molecular machines is an important topic.[1] Mechanically interlocked molecules (MIMs) such as switchable rotaxanes are capable of performing work on the molecular level through structural changes initiated by external stimuli.[2] These stimuli can be of chemical, photochemical, or electrochemical nature.[3] In solution, however, molecular devices are distributed randomly, without any directional control. Depositing them on solid supports in large ordered arrays would therefore provide the basis for a concerted movement. Furthermore, oriented layers would lead to a maximum amount of deposited molecules and thus could help to maximize the effect of molecular movement. Thus, the controlled transfer of molecular switches from solution to surfaces is of great importance in this field.[4] Several reports exist concerning the deposition of interlocked molecular systems;[5] but only very few reports on the successful deposition of tetralactam macrocycles and rotaxanes are available so far.[6] To the best of our knowledge, no example exists that shows a preferential orientation of interlocked molecules on solid supports in large ordered arrays.[5a]

Self-assembly is required to achieve ordered arrays of supramolecules, because error correction requires reversible deposition processes to operate, for which noncovalent interactions are favorable. Also, a preordered template layer as realized in self-assembled monolayers (SAMs)[7] with suitable terminal groups is preferable to help induce order in the adlayer deposited on top of the SAM. The connection between a SAM and a supramolecule adlayer can be accomplished by metal-to-ligand coordination using pyridines or terpyridines.[7a,8] These ligands are known to form long-lived and robust complexes with transition metals due to strong metal-to-ligand back donation and, for the terpyridine ligands, due to chelating effects.[9]

A number of studies exists using pyridine-terminated SAMs for coordination chemistry on gold substrates.[7a,10] Recently, we investigated a pyridine-substituted alkyl thiol, that is, 12-(pyridine-4-yl)dodecane-1-thiol (PDT, Scheme 1a).[11] The PDT-SAM was shown to be perfectly suitable for the complexation of terpyridines using Pd(II) ions. However, the alkyl backbone of PDT causes the terminal pyridine group to be somewhat flexible with respect to its orientation.

In this study, a novel SAM formed from (*E*)-4-(pyridine-4-yl)stilbenethiol (PST, Scheme 1b) with a rigid stilbene backbone was investigated. The palladium-directed self-assembly of terpyridine functionalized tetralactam macrocycles and rotaxanes[12] on PST and PDT was carried out. Multi-technique analysis using X-ray photoelectron spectroscopy (XPS), time-of-flight secondary-ion mass spectrometry (ToF-SIMS), and near-edge X-ray absorption fine structure

Received: June 26, 2012
Published: September 4, 2012

dx.doi.org/10.1021/ja306212m | *J. Am. Chem. Soc.* 2012, 134, 16289−16297

Scheme 1. (a) SAM Constituent PDT and (b) Synthesis of the New SAM Constituent PST

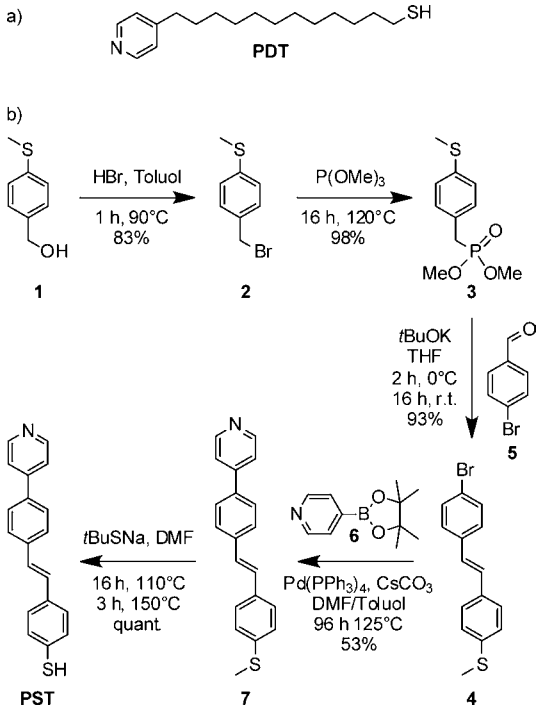

(NEXAFS) spectroscopy was applied to provide evidence for their successful deposition. The deposited macrocycles and rotaxanes were investigated with respect to preferential orientation by angle-resolved NEXAFS spectroscopy. In order to determine whether a template layer with a flexible or a rigid terminal pyridine-group is preferable, the PST- and PDT-SAMs were compared with respect to the amount of deposited macrocycles and of the preferential orientation of macrocycles and rotaxanes. Furthermore, the time required for the self-assembly process was determined. The comparative studies were done by ToF-SIMS, because this technique allows the semiquantitative analysis of a specific molecular species adsorbed on the gold surface.

2. RESULTS AND DISCUSSION

In order to provide a good comparability of the two pyridine SAMs for macrocycle deposition, the new PST molecule was designed to have a length similar to that of PDT. Therefore, a stilbene moiety was introduced as a rigid backbone, replacing the flexible alkyl chain of PDT. For the deposition of ordered supramolecule arrays on these template layers, the quite rigid tetralactam macrocycles and the corresponding benzyl ether rotaxanes were equipped with terpyridine groups. Using Pd(II) ions with a square planar coordination sphere for connecting the macrocycle/rotaxane layer to the underlying SAM can be achieved by precomplexation of the macrocycle or rotaxane with Pd(II) and the subsequent deposition of this complex on the pyridine-terminated template monolayers. The trityl stopper units of the corresponding anion-templated ether rotaxanes were substituted with iodine as labeling atoms to enable a straightforward detection of the deposited rotaxanes through XPS.

2.1. Synthesis. The desired SAM molecule PST was synthesized in five steps from (4-(methylthio)phenyl)methanol **1** (Scheme 1b). Substituent exchange in **1** introduces a bromo group and yields (4-(bromomethyl)phenyl)methylsulfane **2** in 83%, which was further converted into the phosphonate **3** in 98% yield. 4-(4-Bromostyryl)phenyl)methylsulfane **4** was synthesized from **3** with 4-bromobenzaldehyde **5** in a Horner–Wadsworth–Emmons-type reaction (93%).[13] Suzuki coupling of **4** with 4-(4,4,5,5-tetramethyl-1,3,2-dioxaborolan-2-yl)pyridine **6** yielded 4-(4-(4-(methylthio)styryl)phenyl)-pyridine **7**. Final deprotection of **7** generated the surface-active thiol (*E*)-4-(pyridine-4-yl)stilbenethiol PST in quantitative yield.

The terpyridine-substituted tetralactam macrocycle MC was synthesized as reported previously and used for the formation of the corresponding rotaxane Rot (Scheme 2).[12a] Vögtle's anion-templated synthesis provided Rot from the 4-(tris(4-iodophenyl)methyl)phenol stopper **8** and the commercially available 1,4-bis(bromomethyl)benzene axle center piece **9** in 52% yield.[14] Coordination of MC and Rot with palladium ions was carried out using tetrakisacetonitrile-palladium(II)-tetrafluoroborate yielding MC–Pd and Rot–Pd in 81% and 92% yield, respectively. Likely, the fourth coordination site at the metal ion is occupied by one quite weakly bound acetonitrile ligand.

2.2. SAM Preparation and Characterization. SAMs were prepared by immersing the freshly cleaned gold substrates into a 1 mM solution of the desired pyridine-substituted thiols PST or PDT for 24 h (Scheme 3a).[11] The characterization of the PDT-SAM has been reported previously.[11] The new PST-SAM was characterized through multitechnique analysis using ToF-SIMS, XPS, and NEXAFS spectroscopy.

Direct evidence for deposited SAM molecules was obtained by ToF-SIMS through bombardment of the substrates with Bi_3^{2+} primary cluster ions. Due to the relatively mild ionization conditions, intact PST was detected among the secondary ions generated by the bombardment. The additional observation of characteristic PST fragments unambiguously identifies the PST to be assembled on the gold surface (Supporting Information).

Further evidence for the successful assembly of the deposited PST SAMs on gold was obtained from the S 2p, C 1s, and N 1s high-resolution XPS (HRXPS) core level spectra (Supporting Information). In the S 2p spectrum, the photoemission at a binding energy (BE) of 162.0 eV is assigned to the Au–S interface of the SAM.[15] The different carbon species forming the PST molecule are superimposed in the C 1s photopeak around a BE of 285.0 eV. The N 1s spectrum shows a peak at a BE of 398.8 eV that is assigned to the aromatic nitrogen of the pyridine terminated SAM.[11,16]

N K-edge NEXAFS spectroscopy revealed a single resonance for the excitation into a π^* orbital at 398.3 eV that can be assigned to an aromatic nitrogen species. The intensity of this resonance depends on the angle of the incident synchrotron light measured relative to the surface plane (Figure 1a). Therefore, we conclude the pyridine groups to form a layer with preferential orientation on top of the SAM.[17] In Figure 1b, the corresponding angle-dependent NEXAFS spectra of the C K-edge are depicted. Two resonances for the excitation into π^* orbitals are observed at 285.1 and 285.4 eV. The splitting of the π^* resonance is characteristic for pyridine groups.[18] The observed linear dichroism reveals the PST molecules to be preferentially upright oriented on the surface consistent with previously reported, almost perpendicular orientations of stilbene thiolate SAMs.[13,16b,18b,19] This consequently also includes the terminal pyridine ring, which is rigidly attached to the substrate.

dx.doi.org/10.1021/ja306212m | J. Am. Chem. Soc. 2012, 134, 16289–16297

Scheme 2. Synthesis of the Iodine-Labeled Rotaxane Rot and the Palladium Coordinated MC−Pd and Rot−Pd

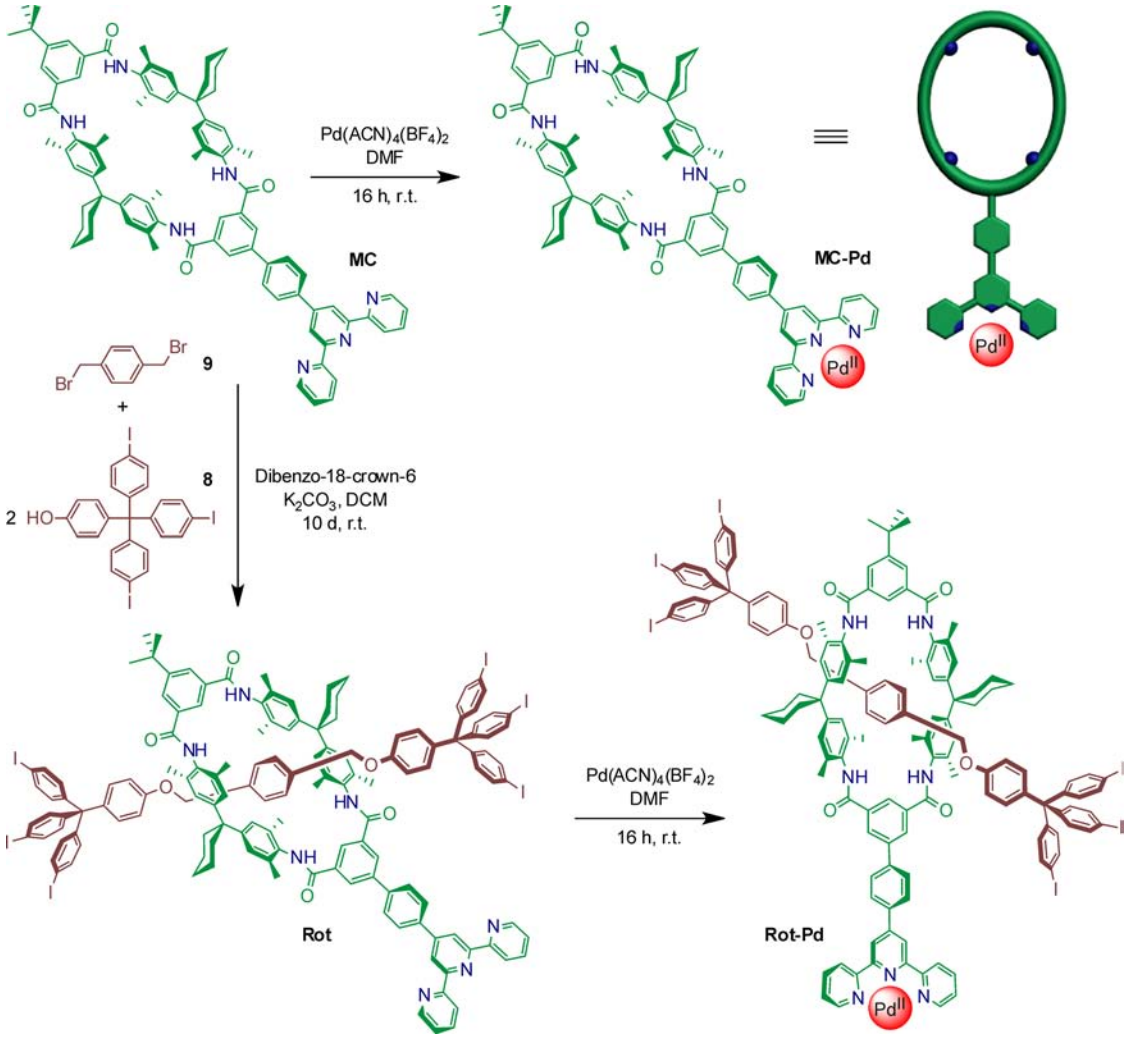

Scheme 3. (a) Preparation of the PST- and PDT-SAMs and (b) Deposition of MC−Pd through Coordination Chemistry Driven Self-Assembly on Pyridine-Terminated PDT- and PST-SAMs

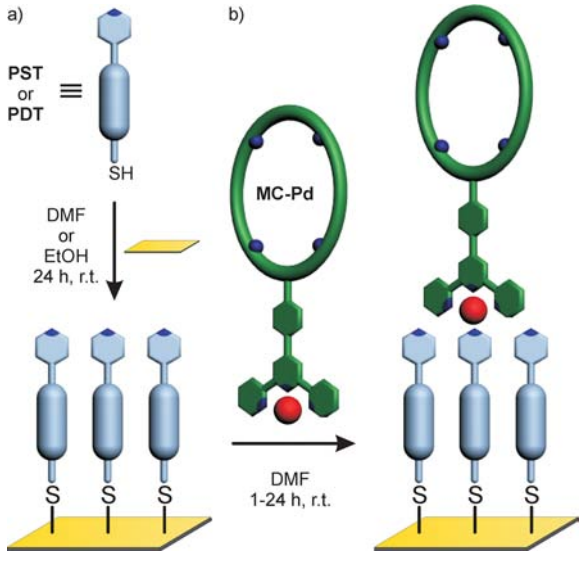

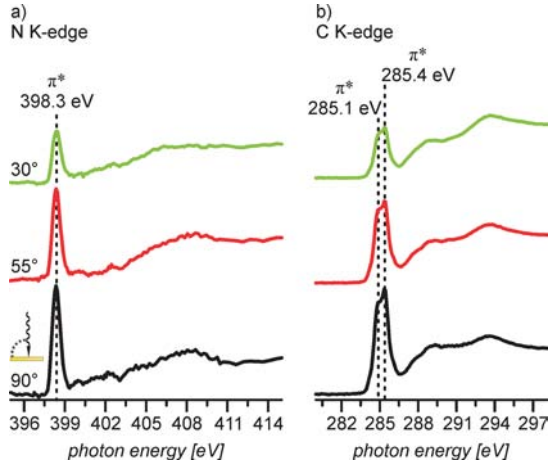

Figure 1. Angle-resolved NEXAFS spectra (in units of normalized PEY (a.u.)) of a PST-SAM: (a) the N K-edge region; (b) the C K-edge region.

In contrast, the terminal pyridine group of the PDT-SAM exhibits no angle dependence in the C K-edge NEXAFS spectrum of the π^* region (Supporting Information), and we conclude that it exists with isotropic orientation at the layer's surface.[11] Consequently, both SAMs exhibit distinctly different

dx.doi.org/10.1021/ja306212m | J. Am. Chem. Soc. 2012, 134, 16289−16297

properties with respect to the orientation and flexibility of the terminal pyridine.

These differences can be expected to have a significant effect on their coordination behavior and therefore to change the surface density and order in the macrocycle and rotaxane adlayer.

2.3. Deposition and Characterization of Macrocycle Layers. Macrocycles were assembled on the pyridine-terminated SAMs by immersing the monolayers into a 1 mM solution of MC−Pd (Scheme 3b). During the self-assembly process, the terminal pyridine groups of the SAM coordinate to the Pd(II) ions and replace the weakly bound acetonitrile ligand of MC−Pd. Thus, the macrocycle is reversibly attached to the surface through coordination chemistry.

Evidence for the deposition of MC−Pd on the PST-SAM is provided by the detection of the typical palladium Pd 3d doublet in the XP spectrum (Figure 2a). The doublet at BEs of

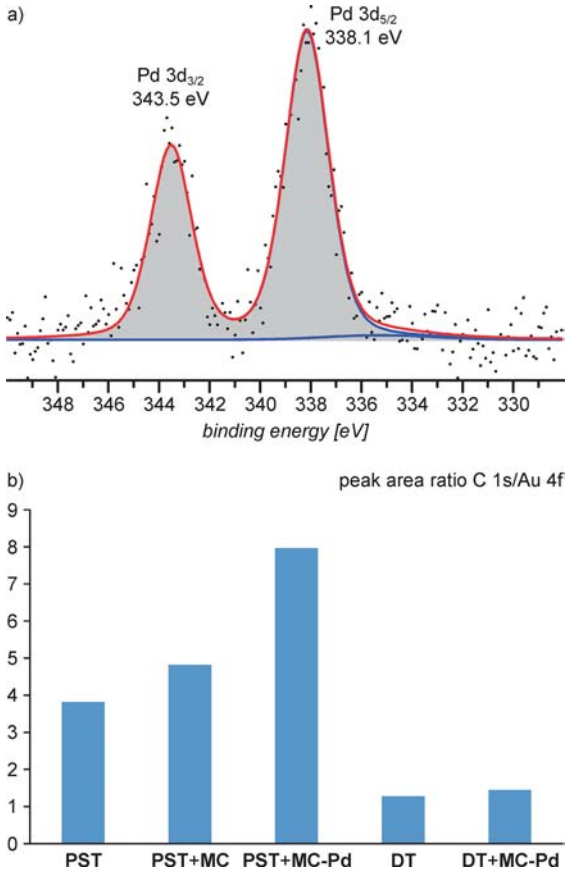

Figure 2. Characterization of deposited MC−Pd on a PST-SAM after 24 h deposition time: (a) Pd 3d core level synchrotron-radiation (SR) XP spectrum (in units of normalized (cps)) at 60° emission angle ($h\nu$ = 500 eV) and (b) peak area ratio C 1s/Au 4f (SR XPS, $h\nu$ = 350 eV) for different surfaces.

338.1 and 343.5 clearly indicates the palladium(II) ions to be coordinated to the pyridines.[11,18a,20] The growth of the organic layer through coordination of MC−Pd on the surface is observed by an increasing peak area ratio C 1s/Au 4f (Figure 2b). While a peak area ratio C 1s/Au 4f of around 4 is observed for the unmodified PST-SAM, the ratio doubles to approximately 8 after the deposition of MC−Pd. In a control experiment, MC−Pd was deposited on a decane-1-thiol (DT) SAM that does not carry any pyridine groups. In this case, no increase of the peak area ratio C 1s/Au 4f is observed. Also, metal-free MC was applied to the PST-SAM under the same experimental conditions. Again, no significant increase of the peak area ratio C 1s/Au 4f is detected. Therefore, the Pd(II) ion is required for the successful deposition of MC providing strong evidence for the coordination of MC−Pd to the pyridine groups of the SAM and excluding unspecific adsorption of the macrocycle on the SAM.

The isotope pattern for $[MC + Pd]^+$ at m/z 1373.58 observed in the ToF-SIMS spectra nicely fits to the calculated one (Figure 3a, b) and thus provides direct evidence for

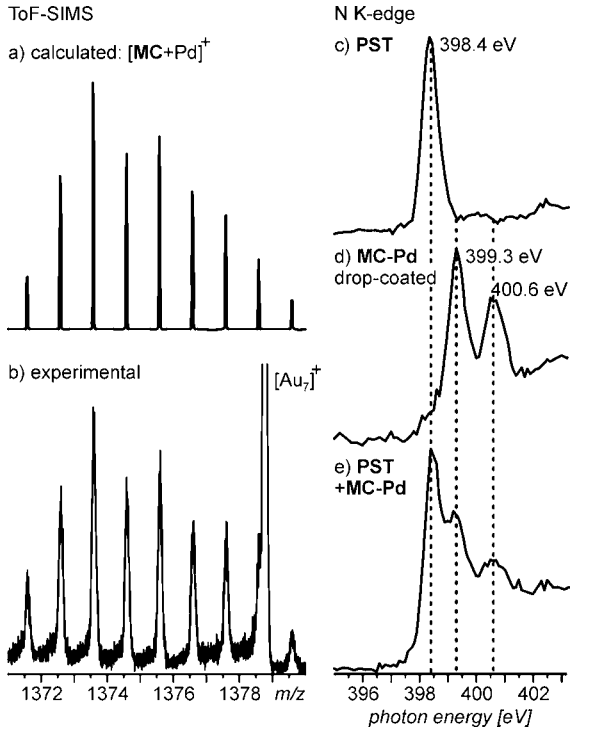

Figure 3. Left: (a) calculated and (b) experimental ToF-SIMS isotope patterns of $[MC + Pd]^+$ (normalized secondary ion yield). Right: NEXAFS N K-edge spectra (in units of normalized PEY (a.u.), 55°) of (c) the PST-SAM, (d) MC−Pd drop-coated on a clean gold surface, and (e) MC−Pd coordinated to the terminal pyridines of the PST-SAM.

deposited macrocycles on the surface. Furthermore, the surface-coordinated macrocycle could also be observed as the $[MC + H]^+$ fragment ion at m/z 1268.68 (Supporting Information).

NEXAFS spectroscopy identifies the deposited MC−Pd through nitrogen resonances in the N K-edge spectra. The unmodified PST-SAM exhibits a single nitrogen resonance feature at 398.4 eV assignable to the uncomplexed pyridine N atoms (Figure 3c). For drop-coated MC−Pd without underlying template SAM, two characteristic resonances are observed at 399.3 and 400.6 eV for palladium-coordinated pyridine and the amide nitrogen atoms, respectively (Figure 3d).[11,18a,21] After coordination of MC−Pd on the PST-SAM, all three resonances appear and reveal the presence of the macrocycle on the surface (Figure 3e). The remaining signal at 398.4 eV indicates the presence of uncomplexed SAM pyridines, which is in line with expectation as the high steric demand of MC makes the coordination of all PST molecules impossible. The analytical data presented here clearly demonstrate the

dx.doi.org/10.1021/ja306212m | J. Am. Chem. Soc. 2012, 134, 16289−16297

successful deposition of MC−Pd on the SAM. Similar results were obtained by using a PDT-SAM (Supporting Information).

Although the coordination of organic ligands to metal ions on solid support is often rather slow,[22] shorter deposition times would be preferable to speed up the surface preparation for future applications. Therefore, we compared the coordination of MC−Pd on a PST-SAM after 1 and 24 h through a quantitative analysis of the amount of deposited macrocycles. For this purpose, NEXAFS N K-edge and ToF-SIMS analyses were used. The two resonances at 399.3 and 400.6 eV in the N K-edge spectra associated to the surface-coordinated macrocycle increase after longer reaction times (Figure 4a). This

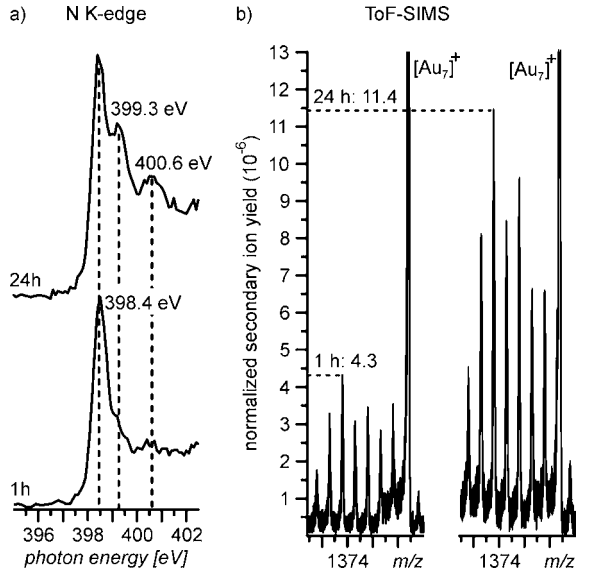

Figure 4. Comparison of the deposition of MC−Pd on a PST-SAM using 1 or 24 h assembly time by (a) NEXAFS N K-edge (in units of normalized PEY (a.u.), 55°) absorption intensities and (b) the normalized secondary ion yield (10^{-6}) of $[MC + Pd]^+$ detected in the ToF-SIMS spectra.

represents a higher amount of deposited macrocycles after 24 h of self-assembly time in contrast to only 1 h. However, the quantitative comparison is quite difficult, because the signals in the N K-edge are a superposition of resonances of different nitrogen species. In contrast, ToF-SIMS allows the detection of single molecular species as separate signals with their specific isotopic patterns and thus can be used to follow the process at least semiquantitatively. All MS spectra were recorded under exactly the same ionization and detection conditions, and the ion intensities were normalized to the total-ion current. For comparison of the amount of macrocycle deposited after different deposition times, the $[MC + Pd]^+$ secondary ion at m/z 1373.58 was chosen (Figure 4b).

The normalized intensity increases from 4.3×10^{-6} to 11.4×10^{-6} indicating that the amount of deposited macrocycle increases significantly between 1 and 24 h deposition time. Consequently, the deposition and self-assembly process needs longer than one hour. This is also supported by the growth of the $[MC + Pd]^+$ ion relative to the $[Au_7]^+$ signal. A similar trend can also be observed by using PDT-SAMs (Supporting Information). Longer deposition times (72 h) did not lead to a significant intensity increase after 24 h indicating the thermodynamic minimum of the self-assembly to be reached within that time frame.

2.4. Comparison of MC Deposition on PST- and PDT-SAMs. ToF-SIMS also allows comparison of the ability of the two SAMs, PDT and PST, to coordinate macrocycles and to determine whether a more flexible or a rigid linker between the Au−S interface and the terminal pyridine is advantageous for the generation of ordered macrocycle layers in terms of surface coverage. The intensities of the $[MC + Pd]^+$ secondary ions, again normalized to the total-ion current, amounts to 11.4×10^{-6} for the deposition of MC−Pd on the monolayer formed from rigid PST, while it is only 6.1×10^{-6} when the more flexible PDT-SAM is used (Figure 5). For both SAMs, very

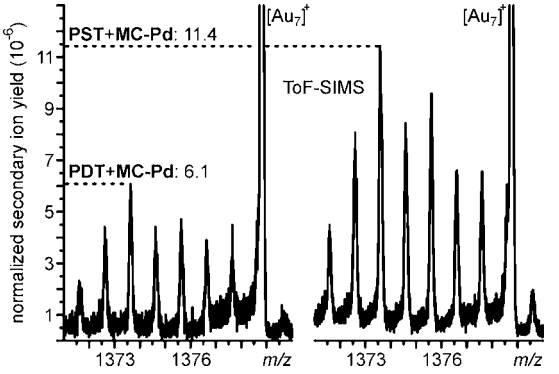

Figure 5. Comparison of the deposition of MC−Pd on a PDT- and PST-SAM expressed by normalized secondary ion yield (10^{-6}) of $[MC + Pd]^+$ detected in the ToF-SIMS spectra.

similar N 1s/Au 4f peak area ratios are obtained by XPS experiments indicating closely similar pyridine densities. The PST-SAM is thus more suitable as a template layer for macrocycle coordination in terms of surface coverage and contains the macrocycle in a more densely packed arrangement. Consequently, the rigidity of the whole PST-molecule comprising spacer and terminal-pyridine group plays an important role for the self-assembly of MC−Pd. We assume that the higher rigidity of the PST molecules causes better preorganization of the pyridines thus orienting the pyridine N atoms away from the surface into a position suitable for coordination of sterically demanding macrocycles.

2.5. Orientation of Deposited Macrocycle Layers. In order to determine a potential preferential orientation of the molecules in the macrocycle layer, angle-resolved C K-edge NEXAFS spectroscopy was applied (Figure 6a). The overall intensities of the two π^* resonances at 285.1 and 285.4 eV increase by increasing incident angles of the synchrotron irradiation as observed for an uncomplexed PST-SAM (Figure 1b). Thus, the preferential upright orientation of the SAM molecules is not affected by the coordination of MC−Pd. Nevertheless, the shape of the π^* resonances changes in contrast to the pristine PST-SAM. While the resonance at 285.1 eV is more intense at an incident angle of 30°, the resonance at 285.4 eV is the dominant signal at 90° angle of incidence. However, the intensity ratio of both resonances reverses by changing the angle of the incident light. This specific linear dichroism effect cannot be assigned to the SAM template, as it is not observed in the NEXAFS spectra in Figure 1b. It is therefore a result of the deposition of MC−Pd. For a more explicit presentation of the linear dichroism effect, the two π^* resonances (C1 and C2) in the C K-edge spectra were fitted (Supporting Information). These resonances are also observed for (ter)pyridyl groups.[18] However, a straightforward assign-

dx.doi.org/10.1021/ja306212m | J. Am. Chem. Soc. 2012, 134, 16289−16297

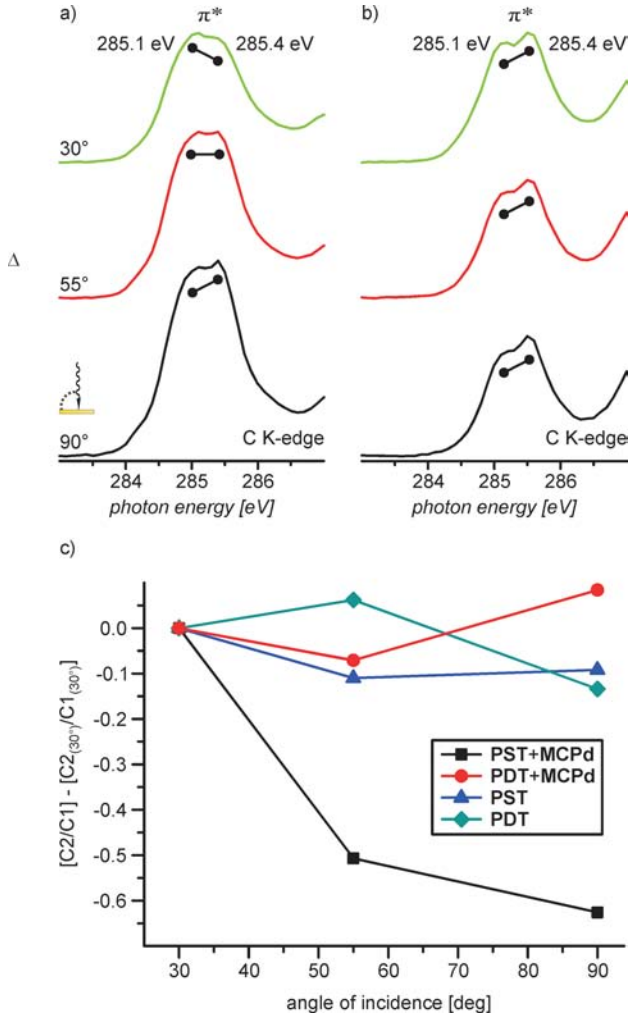

Figure 6. Top: angle-resolved NEXAFS C K-edge spectra (in units of normalized PEY (a.u.)) of the π^* regions of the MC−Pd coordinated to (a) the PST-SAM and (b) the PDT-SAM. Bottom: (c) differences of C2/C1 peak area ratios of π^* resonances between 281 and 286.5 eV at different incident angles of synchrotron light for PST, PDT, PST + MC−Pd, and PDT + MC−Pd surfaces.

ment to specific carbons is not easily possible because of the large number of additional aromatic rings in the macrocycle structure. The change of the peak area ratio C2/C1 is plotted over the angle of the incident light vector in Figure 6c. While for pristine PST- and PDT-SAMs no change is observed, the peak area ratio C2/C1 changes significantly between incident angles of 30° and 90° after the deposition of MC−Pd on a PST-SAM. This underlines the occurrence of specific linear dichroism as a result of MC−Pd coordination on the SAM.

It should be noted that such a rather small linear dichroism effect does not necessarily indicate low order in the macrocycle or, see below, the rotaxane layer. Looking at the molecular structure of the macrocycle, it becomes clear that these molecules contain aromatic rings in a number of different orientations, even when well-ordered. Consequently, even for an ordered array, only small linear dichroism effects would be expected.[23] Although azimuthal disorder cannot rigorously be ruled out, we conclude the long axis of the tetralactam macrocycles to be oriented preferentially upright.

Very interestingly, the corresponding NEXAFS spectra obtained for MC−Pd deposited on the PDT-SAM do not show an analogous specific linear dichroism effect and therefore no change in the peak area ratio C2/C1 at different incident angles (Figure 6b, c). This indicates that orientational order within the macrocycle layer is only obtained when the underlying SAM acts as a true template and by virtue of its rigidity guides the macrocycles into the ordered arrangement. With the more flexible terminal pyridines in the PDT-SAM, this order is lost. These results nicely correspond to the differences in surface coverage of both layers, and we conclude the PST-SAM to template order generation within the macrocycle layer, while the PDT-SAM does not.

2.6. Deposition of Benzyl Ether Rotaxanes. After successful macrocycle deposition, the same procedure was applied to the corresponding benzyl ether rotaxane Rot. The characterization becomes more challenging due to additional carbon and oxygen species of the axle, which for example, are superimposed with other carbon and oxygen signals in the XPS spectra. Also, it was not clear a priori, whether the rotaxane would survive the ToF-SIMS ionization conditions. Pronounced fragmentation of the axle might rather lead to the disappearance of the $[Rot + Pd]^+$ signals so that an unambiguous detection of the rotaxane would be more difficult than that of the macrocycle. Therefore, iodine substituents were introduced into the trityl phenol stopper groups as labels to simplify the analysis of surface-coordinated rotaxanes, which can then be detected by I 3d core level XPS. Additionally, NEXAFS spectroscopy and peak area ratio C 1s/Au 4f C/Au ratios were used for the characterization of deposited rotaxanes.

After 24 h deposition time of Rot−Pd on a PST-SAM, an I 3d doublet at a BEs of 621.1 and 632.7 eV was indeed detected (Figure 7a),[24] which provides evidence for the successful deposition of the labeled rotaxane. The minor species at smaller BE becomes more prominent with rising irradiation time and is

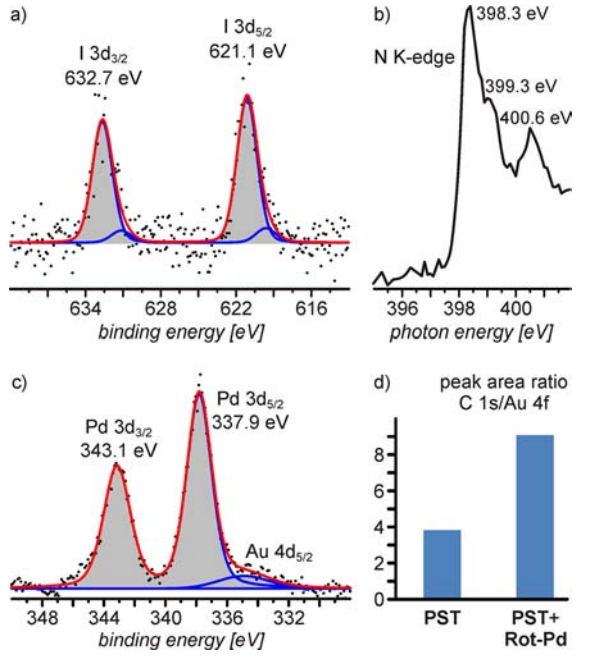

Figure 7. Deposition of Rot−Pd on a PST-SAM detected by (a) an I 3d doublet in the SR XP core level spectrum (in units of normalized (cps)) at 60° emission angle ($h\nu$ = 780 eV), (b) NEXAFS of the N K-edge (in units of normalized PEY (a.u.), 55°), (c) Pd 3d core level SR XP spectrum (in units of normalized (cps)) at 0° emission angle ($h\nu$ = 500 eV), and (d) peak area ratio C 1s/Au 4f (SR XPS, $h\nu$ = 350 eV).

dx.doi.org/10.1021/ja306212m | J. Am. Chem. Soc. 2012, 134, 16289−16297

therefore assigned to inorganic iodine formed by irradiation damage. Additional evidence for the successful deposition of Rot comes from the NEXAFS N K-edge spectrum. Figure 7b shows two nitrogen species at 399.3 and 400.6 eV representing the rotaxane's wheel as described above (Figure 3e). As previously described for the deposition of MC−Pd, Pd(II) photoemission signals were detected revealing successful complex formation (Figure 7c). As expected, the peak area ratio C 1s/Au 4f increases through deposition of the rotaxane (Figure 7d). Similar results were obtained by using a PDT-SAM (Supporting Information).

The order within the rotaxane layer was again analyzed by angle-resolved NEXAFS C K-edge measurements (Figure 8). A

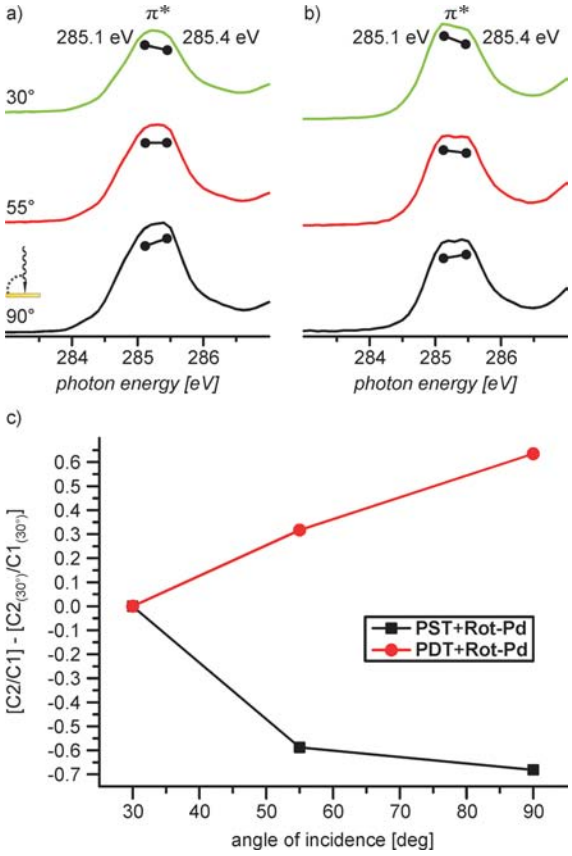

Figure 8. Top: region of the π^* resonances of the angle-resolved NEXAFS C K-edge spectra (in units of normalized PEY (a.u.)) of Rot−Pd coordinated on (a) a PST-SAM and (b) a PDT-SAM. Bottom: (c) differences of C2/C1 peak area ratios of π^* resonances between 281 and 286.5 eV at different incident angles for PST + Rot−Pd and PDT + Rot−Pd surfaces.

small, but clearly detectable linear dichroism effect is observed after coordination of Rot−Pd to both the PST-SAM (Figure 8a) as well as the PDT-SAM (Figure 8b). This is again demonstrated more clearly by the change in the peak area ratio C2/C1 using different angles of incidence of the synchrotron light (Figure 8c). As the macrocycles, the rotaxane wheels are oriented preferentially upright. It is however impossible to assign orientational order to the rotaxane axles based on these data. In contrast to the macrocycles, the rotaxanes obviously pack sufficiently well through lateral interactions on both SAMs to yield ordered arrays irrespective of the template's backbone rigidity and the flexibility of the terminal SAM pyridine groups. For efficient lateral interactions, rather densely packed layers are required. The packing density was estimated from N 1s XPS data (for details, see the Supporting Information). About 15−20% of the available SAM pyridines are coordinated to Rot−Pd molecules in reasonable agreement with the dimensions of the rotaxanes in a preferentially upright orientation.

3. CONCLUSIONS

In this study, the deposition of supramolecules on two different pyridine-terminated template layers was investigated. Quite densely packed and ordered SAMs consisting of either PDT or the new PST were deposited on gold substrates and investigated by multitechnique analysis. The terminal pyridine of PST is highly ordered whereas PDT contains a more flexible terminal-pyridine group. These two SAMs were used as substrates for the self-assembly of ordered metal-coordinated tetralactam macrocycles MC−Pd and rotaxanes Rot−Pd. A combination of XPS, NEXAFS, and ToF-SIMS permits the unambiguous identification of the surface-deposited macrocycles MC−Pd and the corresponding rotaxanes Rot−Pd. To investigate the time dependence of the self-assembly of MC−Pd, ToF-SIMS analysis was applied and furthermore used to determine which of the two template layers is more suitable for the coordination of MC−Pd. PST was found to be preferable due to the more rigid terminal pyridine groups.

Angle-resolved NEXAFS experiments of the C K-edge reveal a preferential upright orientation of the supramolecules on the surface. Besides the rigidity of the template SAM, subtle details of the lateral interactions between adjacent macrocycles or rotaxanes govern the generation of order: while ordered macrocycles were only observed on the more rigid PST-SAM, but not on the PDT monolayer, the rotaxanes are ordered on both substrates. The template effect caused by the rigidity of the underlying monolayer is thus more important for the ordered deposition of macrocycles than rotaxanes. The generation of ordered rotaxane layers on the PDT-SAM is nevertheless possible when rotaxanes Rot−Pd sufficiently self-pack. In this case, the order in the rotaxane adlayer induces preferential orientation of the previously unordered terminal pyridines of the PDT molecules.

The metal-mediated coordination of tetralactam macrocycles and the corresponding benzyl ether rotaxanes to the pyridine-terminated SAMs presented here is well-suited for the deposition of ordered supramolecular arrays on solid supports and may become a valuable tool in the future for depositing molecular machines and mechanically interlocked switches to surfaces that are ready for concerted action and potentially exert macroscopic effects. One important question for realizing such layers with functional supramolecules will be whether concerted switching or motion is possible at all in densely packed layers. Potentially, such functionality might require a delicate balance between organization and packing. The present study lays the foundation to answer this question when switchable rotaxanes become available for deposition in the future.

■ ASSOCIATED CONTENT

Ⓢ Supporting Information

Full experimental procedures and characterization of new compounds and surfaces; copies of ^{1}H, ^{13}C, ^{19}F, and ^{31}P NMR spectra; NMR study of the formation of Rot; instrumentation and data processing used for the described experiments; additional XPS, NEXAFS, and ToF-SIMS data for the characterization of the novel PST-SAM and the deposited

MC−Pd and Rot−Pd on PST and PDT; peak fit of the C K edge-NEXAFS π^* regions; details on estimation of packing density; and references. This material is available free of charge via the Internet at http://pubs.acs.org.

AUTHOR INFORMATION

Corresponding Author

c.schalley@schalley-lab.de; wolfgang.unger@bam.de

Notes

The authors declare no competing financial interest.

ACKNOWLEDGMENTS

The authors gratefully acknowledge the Deutsche Forschungsgemeinschaft (SCHA 893/9-1, UN 80/8-1), the Freie Universität Berlin, and the Fonds der Chemischen Industrie (FCI) for financial support. S.R. thanks the FCI for a Chemiefonds Ph.D. fellowship. We are grateful to Th. Wirth and D. Treu for operating the ToF-SIMS and XPS instruments, respectively, at BAM 6.8. We thank B. Baytekin for fruitful discussions and A. Schulz for AFM measurements. Support by A. Lippitz (BAM), A. Nefedov (KIT), and staff at BESSY II (Dr. W. Braun, Dr. G. Reichardt, and M. Mast) during our activities at the HESGM beamline is gratefully acknowledged.

REFERENCES

(1) (a) Feringa, B. L. *Acc. Chem. Res.* **2001**, *34*, 504−513. (b) Kay, E. R.; Leigh, D. A. *Top. Curr. Chem.* **2005**, *262*, 133−177. (c) Coskun, A.; Banaszak, M.; Astumian, R. D.; Stoddart, J. F.; Grzybowski, B. A. *Chem. Soc. Rev.* **2012**, *41*, 19−30. (d) Eelkema, R.; Pollard, M. M.; Vicario, J.; Katsonis, N.; Ramon, B. S.; Bastiaansen, C. W. M.; Broer, D. J.; Feringa, B. L. *Nature* **2006**, *440*, 163−163. (e) Carroll, G. T.; London, G.; Landaluce, T. F.; Rudolf, P.; Feringa, B. L. *ACS Nano* **2011**, *5*, 622−630. (f) Kudernac, T.; Ruangsupapichat, N.; Parschau, M.; Macia, B.; Katsonis, N.; Harutyunyan, S. R.; Ernst, K.-H.; Feringa, B. L. *Nature* **2011**, *479*, 208−211. (g) Ambrogio, M. W.; Thomas, C. R.; Zhao, Y.-L.; Zink, J. I.; Stoddart, J. F. *Acc. Chem. Res.* **2011**, *44*, 903−913. (h) Avellini, T.; Li, H.; Coskun, A.; Barin, G.; Trabolsi, A.; Basuray, A. N.; Dey, S. K.; Credi, A.; Silvi, S.; Stoddart, J. F.; Venturi, M. *Angew. Chem., Int. Ed.* **2012**, *51*, 1611−1615. (i) Kay, E. R.; Leigh, D. A.; Zerbetto, F. *Angew. Chem., Int. Ed.* **2007**, *46*, 72−191.

(2) (a) Schalley, C. A.; Beizai, K.; Vögtle, F. *Acc. Chem. Res.* **2001**, *34*, 465−476. (b) Olsen, J.-C.; Griffiths, K. E.; Stoddart, J. F. In *From Non-Covalent Assemblies to Molecular Machines*; Sauvage, J.-P., Gaspard, P., Eds.; Wiley-VCH: Weinheim, Germany, 2010; pp 65−139. (c) Brouwer, A. M.; Frochot, C.; Gatti, F. G.; Leigh, D. A.; Mottier, L.; Paolucci, F.; Roffia, S.; Wurpel, G. W. H. *Science* **2001**, *291*, 2124−2128. (d) Panman, M. R.; Bodis, P.; Shaw, D. J.; Bakker, B. H.; Newton, A. C.; Kay, E. R.; Leigh, D. A.; Buma, W. J.; Brouwer, A. M.; Woutersen, S. *Phys. Chem. Chem. Phys.* **2012**, *14*, 1865−1875. (e) Balzani, V.; Credi, A.; Venturi, M. In *From Non-Covalent Assemblies to Molecular Machines*; Sauvage, J.-P., Gaspard, P., Eds.; Wiley-VCH: Weinheim, Germany, 2010; pp 157−212. (f) Badjic, J. D.; Ronconi, C. M.; Stoddart, J. F.; Balzani, V.; Silvi, S.; Credi, A. *J. Am. Chem. Soc.* **2006**, *128*, 1489−1499. (g) Garaudée, S.; Silvi, S.; Venturi, M.; Credi, A.; Flood, A. H.; Stoddart, J. F. *Chem. Phys. Chem.* **2005**, *6*, 2145−2152.

(3) (a) Balzani, V.; Credi, A.; Raymo, F. M.; Stoddart, J. F. *Angew. Chem., Int. Ed.* **2000**, *39*, 3348−3391. (b) Ballardini, R.; Balzani, V.; Credi, A.; Gandolfi, M. T.; Venturi, M. *Acc. Chem. Res.* **2001**, *34*, 445−455. (c) Li, H.; Fahrenbach, A. C.; Coskun, A.; Zhu, Z.; Barin, G.; Zhao, Y.-L.; Botros, Y. Y.; Sauvage, J.-P.; Stoddart, J. F. *Angew. Chem., Int. Ed.* **2011**, *50*, 6674−6674. (d) Balzani, V.; Credi, A.; Venturi, M. *Chem. Soc. Rev.* **2009**, *38*, 1542−1550. (e) Carlone, A.; Goldup, S. M.; Lebrasseur, N.; Leigh, D. A.; Wilson, A. *J. Am. Chem. Soc.* **2012**, *134*, 8321−8323. (f) Durola, F.; Lux, J.; Sauvage, J.-P.; Wenger, O. S. *Supramol. Chem.* **2010**, *23*, 42−52.

(4) (a) Balzani, V.; Credi, A.; Venturi, M. *Chem. Phys. Chem.* **2008**, *9*, 202−220. (b) Boyle, M. M.; Smaldone, R. A.; Whalley, A. C.; Ambrogio, M. W.; Botros, Y. Y.; Stoddart, J. F. *Chem. Sci.* **2011**, *2*, 204−210. (c) Fioravanti, G.; Haraszkiewicz, N.; Kay, E. R.; Mendoza, S. M.; Bruno, C.; Marcaccio, M.; Wiering, P. G.; Paolucci, F.; Rudolf, P.; Brouwer, A. M.; Leigh, D. A. *J. Am. Chem. Soc.* **2008**, *130*, 2593−2601. (d) Juluri, B. K.; Kumar, A. S.; Liu, Y.; Ye, T.; Yang, Y.-W.; Flood, A. H.; Fang, L.; Stoddart, J. F.; Weiss, P. S.; Huang, T. J. *ACS Nano* **2009**, *3*, 291−300. (e) Nguyen, T. D.; Tseng, H.-R.; Celestre, P. C.; Flood, A. H.; Liu, Y.; Stoddart, J. F.; Zink, J. I. *Proc. Natl. Acad. Sci. U.S.A.* **2005**, *102*, 10029−10034.

(5) (a) Davis, J. J.; Orlowski, G. A.; Rahman, H.; Beer, P. D. *Chem. Commun.* **2010**, *46*, 54−63. (b) Coronado, E.; Gavina, P.; Tatay, S. *Chem. Soc. Rev.* **2009**, *38*, 1674−1689. (c) Berná, J.; Leigh, D. A.; Lubomska, M.; Mendoza, S. M.; Pérez, E. M.; Rudolf, P.; Teobaldi, G.; Zerbetto, F. *Nat. Mater.* **2005**, *4*, 704−710. (d) Collier, C. P.; Jeppesen, J. O.; Luo, Y.; Perkins, J.; Wong, E. W.; Heath, J. R.; Stoddart, J. F. *J. Am. Chem. Soc.* **2001**, *123*, 12632−12641. (e) Zhao, L.; Davis, J. J.; Mullen, K. M.; Chmielewski, M. J.; Jacobs, R. M. J.; Brown, A.; Beer, P. D. *Langmuir* **2009**, *25*, 2935−2940. (f) Klajn, R.; Fang, L.; Coskun, A.; Olson, M. A.; Wesson, P. J.; Stoddart, J. F.; Grzybowski, B. A. *J. Am. Chem. Soc.* **2009**, *131*, 4233−4235. (g) Katz, E.; Lioubashevsky, O.; Willner, I. *J. Am. Chem. Soc.* **2004**, *126*, 15520−15532. (h) Katz, E.; Sheeney-Haj-Ichia, L.; Willner, I. *Angew. Chem., Int. Ed.* **2004**, *116*, 3354−3362. (i) Tseng, H.-R.; Wu, D.; Fang, N. X.; Zhang, X.; Stoddart, J. F. *Chem. Phys. Chem* **2004**, *5*, 111−116.

(6) De Nadaï, C.; Whelan, C. M.; Perollier, C.; Clarkson, G.; Leigh, D. A.; Caudano, R.; Rudolf, P. *Surf. Sci.* **2000**, *454−456*, 112−117.

(7) (a) Altman, M.; Shukla, A. D.; Zubkov, T.; Evmenenko, G.; Dutta, P.; van der Boom, M. E. *J. Am. Chem. Soc.* **2006**, *128*, 7374−7382. (b) Hatzor, A.; Moav, T.; Cohen, H.; Matlis, S.; Libman, J.; Vaskevich, A.; Shanzer, A.; Rubinstein, I. *J. Am. Chem. Soc.* **1998**, *120*, 13469−13477. (c) Zacher, D.; Schmid, R.; Wöll, C.; Fischer, R. A. *Angew. Chem., Int. Ed.* **2011**, *50*, 176−199.

(8) (a) Kurita, T.; Nishimori, Y.; Toshimitsu, F.; Muratsugu, S.; Kume, S.; Nishihara, H. *J. Am. Chem. Soc.* **2010**, *132*, 4524−4525. (b) Tuccitto, N.; Delfanti, I.; Torrisi, V.; Scandola, F.; Chiorboli, C.; Stepanenko, V.; Würthner, F.; Licciardello, A. *Phys. Chem. Chem. Phys.* **2009**, *11*, 4033−4038. (c) Tuccitto, N.; Ferri, V.; Cavazzini, M.; Quici, S.; Zhavnerko, G.; Licciardello, A.; Rampi, M. A. *Nat. Mater.* **2009**, *8*, 41−46.

(9) Schubert, U. S.; Hofmeier, H.; Newkome, G. R. *Modern Terpyridine Chemistry*, 1st ed.; Wiley-VCH: Weinheim, Germany, 2006.

(10) (a) Silien, C.; Lahaye, D.; Caffio, M.; Schaub, R.; Champness, N. R.; Buck, M. *Langmuir* **2011**, *27*, 2567−2574. (b) Zhou, W.; Baunach, T.; Ivanova, V.; Kolb, D. M. *Langmuir* **2004**, *20*, 4590−4595.

(11) Poppenberg, J.; Richter, S.; Darlatt, E.; Traulsen, C. H. H.; Min, H.; Unger, W. E. S.; Schalley, C. A. *Surf. Sci.* **2012**, *606*, 367−377.

(12) (a) Baytekin, B.; Zhu, S. S.; Brusilowskij, B.; Illigen, J.; Ranta, J.; Huuskonen, J.; Russo, L.; Rissanen, K.; Kaufmann, L.; Schalley, C. A. *Chem.—Eur. J.* **2008**, *14*, 10012−10028. (b) Hunter, C. A. *J. Am. Chem. Soc.* **1992**, *114*, 5303−5311. (c) Vögtle, F.; Meier, S.; Hoss, R. *Angew. Chem., Int. Ed.* **1992**, *31*, 1619−1622.

(13) Malicki, M.; Guan, Z.; Ha, S. D.; Heimel, G.; Barlow, S.; Rumi, M.; Kahn, A.; Marder, S. R. *Langmuir* **2009**, *25*, 7967−7975.

(14) (a) Schalley, C. A.; Weilandt, T.; Brüggemann, J.; Vögtle, F. *Top. Curr. Chem.* **2004**, *248*, 285−295. (b) Schalley, C. A.; Silva, G.; Nising, C. F.; Linnartz, P. *Helv. Chim. Acta* **2002**, *85*, 1578−1596. (c) Ghosh, P.; Mermagen, O.; Schalley, C. A. *Chem. Commun.* **2002**, 2628−2629. (d) Schalley, C., Baytekin, H., Baytekin, B., Gloe, K., Eds.; Springer: The Netherlands, 2005; pp 37−52. (e) Hübner, G. M.; Gläser, J.; Seel, C.; Vögtle, F. *Angew. Chem., Int. Ed.* **1999**, *38*, 383−386. (f) Seel, C.; Vögtle, F. *Chem.—Eur. J.* **2000**, *6*, 21−24. (g) Reuter, C.; Schmieder, R.; Vögtle, F. *Pure Appl. Chem.* **2000**, *72*, 2233−2241.

(15) Vericat, C.; Vela, M. E.; Benitez, G.; Carro, P.; Salvarezza, R. C. *Chem. Soc. Rev.* **2010**, *39*, 1805−1834.

(16) (a) Silien, C.; Buck, M.; Goretzki, G.; Lahaye, D.; Champness, N. R.; Weidner, T.; Zharnikov, M. *Langmuir* **2008**, *25*, 959−967.

(b) Zubavichus, Y.; Zharnikov, M.; Yang, Y.; Fuchs, O.; Umbach, E.; Heske, C.; Ulman, A.; Grunze, M. *Langmuir* **2004**, *20*, 11022−11029.
(17) Stöhr, J. *NEXAFS Spectroscopy*; Springer: Heidelberg, Germany, 1992.
(18) (a) Darlatt, E.; Traulsen, C. H. H.; Poppenberg, J.; Richter, S.; Kühn, J.; Schalley, C. A.; Unger, W. E. S. *J. Electron Spectrosc. Relat. Phenom.* **2012**, *185*, 85−89. (b) Liu, J.; Schüpbach, B.; Bashir, A.; Shekhah, O.; Nefedov, A.; Kind, M.; Terfort, A.; Wöll, C. *Phys. Chem. Chem. Phys.* **2010**, *12*, 4459−4472. (c) Hamoudi, H.; Döring, K.; Chesneau, F.; Lang, H.; Zharnikov, M. *J. Phys. Chem. C* **2011**, *116*, 861−870.
(19) Mondal, P. C.; Yekkoni Lakshmanan, J.; Hamoudi, H.; Zharnikov, M.; Gupta, T. *J. Phys. Chem. C* **2011**, *115*, 16398−16404.
(20) Brant, P.; Benner, L. S.; Balch, A. L. *Inorg. Chem.* **1979**, *18*, 3422−3427.
(21) Baugh, L.; Weidner, T.; Baio, J. E.; Nguyen, P.-C. T.; Gamble, L. J.; Stayton, P. S.; Castner, D. G. *Langmuir* **2010**, *26*, 16434−16441.
(22) Greenstein, M.; Ben Ishay, R.; Maoz, B. M.; Leader, H.; Vaskevich, A.; Rubinstein, I. *Langmuir* **2010**, *26*, 7277−7284.
(23) Samuel, N. T.; Lee, C.-Y.; Gamble, L. J.; Fischer, D. A.; Castner, D. G. *J. Electron Spectrosc. Relat. Phenom.* **2006**, *152*, 134−142.
(24) Proven by powder XPS of iodine substituted rotaxanes showing the same BE of the I 3d doublet.